Combination of *in-situ* ion beam analysis and thermal desorption spectroscopy for studying deuterium implanted in tungsten

To cite this article: K Kantre *et al* 2021 *Phys. Scr.* **96** 124004

View the article online for updates and enhancements.

Physica Scripta

PAPER

Combination of *in-situ* ion beam analysis and thermal desorption spectroscopy for studying deuterium implanted in tungsten

K Kantre[1] , P S Szabo[2] , M V Moro[1] , C Cupak[2] , R Stadlmayr[2] , L Zendejas Medina[3] , F Aumayr[2] and D Primetzhofer[1]

1 Department of Physics and Astronomy, Uppsala University, Box 516, S-751 20 Uppsala, Sweden
2 Institute of Applied Physics, TU Wien, Fusion@ÖAW, Wiedner Hauptstrasse 8-10/E134, 1040 Vienna, Austria
3 Department of Chemistry, Uppsala University, Box 538, S-751 21 Uppsala, Sweden

E-mail: daniel.primetzhofer@physics.uu.se

Abstract

We demonstrate a combinatorial approach integrating ion implantation followed by thermal annealing and simultaneous *in situ* ion beam analysis with thermal desorption spectroscopy in a single set-up. Atomic and molecular deuterium ions of 3 keV were implanted into bulk tungsten with doses exceeding 1×10^{22} ions m^{-2}. Depth profiling of both, protium and deuterium was performed by elastic recoil detection analysis, while simultaneously the outgassing rates of molecular deuterium by thermal desorption spectroscopy were monitored during temperature ramps from room temperature to $\approx$1400 K. The combination of the two techniques *in situ* is shown capable to identify the distinct retention behavior of deuterium at different temperatures and in different reservoirs, e.g. located close to the surface and diffused deep into the material. *Ex-situ* scanning electron microscopy confirmed blister formation, and recovery of the initial surface morphology after high temperature annealing, in analogy to comprehensive *ex-situ* studies.

1. Introduction

Understanding plasma-wall interactions is essential for effective operation of fusion devices [1–3]. Plasma-facing components (PFCs) are heavily modified as wall materials are continuously eroded and redeposited, forming a mixed layer [4]. Additionally, charge exchange neutrals as well as ions drifting across the scrape-off layer are escaping the plasma and are implanted in the walls, which enhances erosion by sputtering and affects the fuel cycle [5].

This highly challenging environment as well as different aspects of plasma physics lead to specific desirable characteristics of PFCs. For this purpose, several materials have been tested. Presently, two main candidates to be used in next generation fusion research reactors walls are tungsten and beryllium with extensive studies performed on the retention of hydrogen isotopes in these materials [6, 7]. Tungsten, which will be used for the ITER divertor [8], has a very high melting temperature (3695 K), low sputtering yield [9, 10] and exhibits a very low solubility of hydrogen isotopes [6]. The retention of deuterium in tungsten has been studied either by using samples obtained directly from tokamak PFCs [11] or deuterium loaded samples in laboratory conditions, i.e. by plasma exposure [12, 13], ion implantation [14, 15] or exposure to neutral atoms [16].

In this context, Ion Beam Analysis (IBA) techniques have proven to be powerful tools in analyzing plasma-exposed components from fusion reactors, as they offer near surface depth profiling and quantification capabilities [17]. Nuclear Reaction Analysis (NRA) and Elastic Recoil Detection Analysis (ERDA) are used in most IBA studies of plasma facing components, as they exhibit high isotope and light element sensitivity. At the same time, Thermal Desorption Spectroscopy (TDS) has been widely used to measure outgassing rates and trapping energies of hydrogen in materials [18] as well as in fusion related research for studying retention of

hydrogen isotopes in plasma facing components [19, 20]. TDS has also been specifically used to identify potential trapping sites of deuterium in tungsten [21, 22].

A correlation of data obtained by TDS to quantitative depth profiles from IBA is of interest, as a Residual Gas Analyzer (RGA) can be operated even in the challenging conditions of a fusion reactor [23], but does not provide information on the depth distribution and spatial dynamics of implanted species in the PFCs at elevated temperatures. Moreover, sample transport between different set-ups used for plasma exposure or ion implantation and analysis during annealing often involves sample exposure to ambient conditions. This procedure alters surface properties of the samples by the formation of oxide layers, which can act as a near-surface diffusion barrier [24]. In this context, experimental set-ups that enable *in situ* ion implantation, IBA and TDS have been developed [25] and first studies that combine IBA and TDS to investigate the retention of hydrogen isotopes in fusion related materials have been performed [26, 27].

In this manuscript, we present a further application of this approach to study deuterium and hydrogen retention in tungsten *in-situ* by combining ion implantation with real-time IBA characterization during a TDS experiment in a single system. Deuterium ions were implanted in tungsten samples and annealed *in-situ*, while the evolution of the near-surface deuterium content of the samples was tracked by ERDA using foil absorbers supported by PIXE analysis. Simultaneously, the cumulative deuterium release of the sample was recorded by TDS, enabling us to correlate IBA results to data from TDS, and to disentangle the contribution from all expected deuterium reservoirs.

2. Experimental procedure

Polycrystalline tungsten bulk foils of $\approx 10 \times 10$ mm^2 and 0.5 mm thickness commercially available from MaTecK GmbH (nominal purity of 99.9%) were used for the presented investigations. The samples were ultrasonically cleaned in distilled water and isopropyl alcohol (99%). After cleaning, sample surface and bulk chemical composition were investigated by *ex-situ* ion beam analysis using coincidence Time-of-Flight/Energy Elastic Recoil Detection Analysis (ToF-E ERDA) with 36 MeV I^{8+} as probing beam at Uppsala University (details of the set-up in [28]). No bulk contaminants were found in the sample (quantification limit of the present technique <0.3 at.%). The root-mean-square (RMS) roughness of the sample surface was found to be ≈ 7 nm investigated by Atomic Force Microscopy (AFM) at TU Wien.

The *in-situ* measurements were performed using the SIGMA system (Set-up for *In-situ* Growth, Material modification and Analysis) [29], coupled to the 5-MV NEC-15SDH-2 Tandem accelerator at Uppsala University [30]. The Ultra-High-Vacuum (UHV) ($<10^{-8}$ mbar) set-up provides the capability of ion implantation using a Prevac IS40 ion source, electron beam sample annealing, non-destructive sample characterization by ion beams and TDS analysis with an RGA.

Atomic and molecular species of deuterium were implanted in tungsten samples at fluences ranging from 1.1×10^{22} D m^{-2} to 1.7×10^{22} D m^{-2}, assuming 7% atomic (D$^+$) and 93% molecular (D$_2^+$) beam [31]. The implantation flux was $\sim 2.5 \times 10^{17}$ D m^{-2} s^{-1} and samples were kept at room temperature during implantation. As reflection of incident species (estimated $\sim 45\%$ by TRI3DYN [32] and $\sim 38\%$ by SRIM [33]) and degassing of samples during irradiation have to be expected, the implanted doses are in the following referred to as 'nominal' doses representing an upper limit of the actual D-content. The accelerating voltage was kept at 3 kV for all implantations and the sample surface was tilted at 4° with respect to surface normal to reduce possible texture effects and associated channeling. The samples were biased at +36 V during implantation to suppress secondary electrons potentially affecting the current measurement. In the following, mainly results of the *in-situ* investigation for a nominal dose of 1.34×10^{22} D m^{-2} are presented and discussed. Complementary *ex-situ* information on surface morphology was obtained from additional implantations on twin samples.

As illustrated in figure 1(a), samples were first implanted by deuterium ions, before they were rotated to a geometry suitable for IBA. The time between commencing implantation and IBA varied between 1 and 20 h, depending on the final dose. ^{4}He^{++} beams of 3400 and 6200 keV were used to perform simultaneous ERDA and Particle Induced x-ray Emission (PIXE) measurements. The incident angle of the ^{4}He^{++} beam was 70° with respect to the surface normal. The beam spot size is approximately 2–3 mm^2. A Passivated Implanted Planar Silicon (PIPS) detector with an energy resolution of 30 keV and a solid angle of $(3.4 \pm 0.1) \times 10^{-3}$ Sr was used for ERDA. For low energy ERDA, the recoil detection angle was 27° with respect to the beam direction and an Al absorber foil of 12.9 μm was mounted in front of the detector to stop scattered primary ions and W recoils. In the case of the high energy beam, detection angle and absorber thickness were 30° and 33 μm, respectively. The specific choice of energy, angle and absorber foil was made to maximize near-surface resolution and to employ well-known cross sections [34, 35]. For 3400 keV ERDA, the depth resolution for protium and deuterium is approximately 40 nm and the information depth is limited to approximately 350 nm. For 6200 keV the information depth is close to 1 μm but depth resolution deteriorates to approximately 140 nm for deuterium.
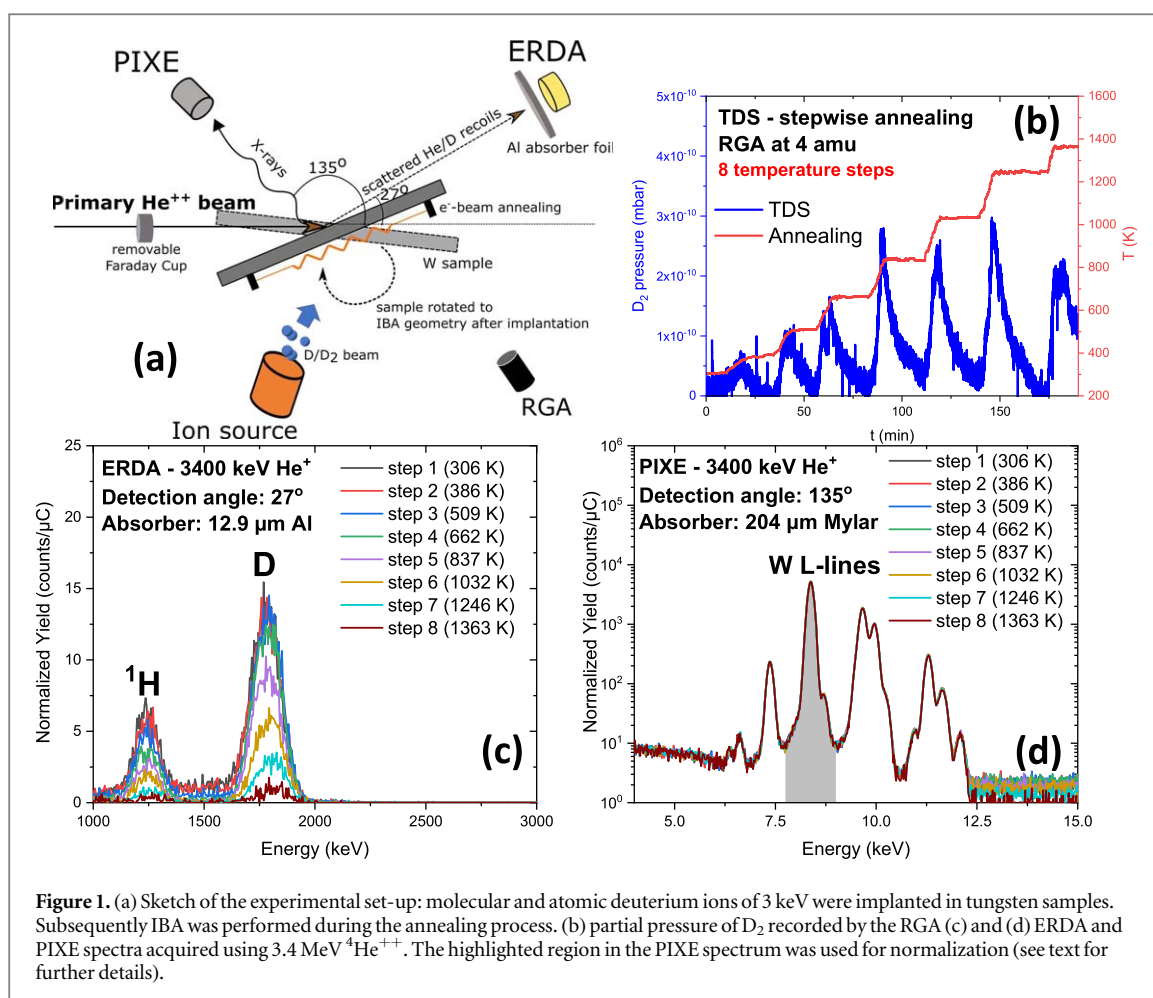
Figure 1. (a) Sketch of the experimental set-up: molecular and atomic deuterium ions of 3 keV were implanted in tungsten samples. Subsequently IBA was performed during the annealing process. (b) partial pressure of D_2 recorded by the RGA (c) and (d) ERDA and PIXE spectra acquired using 3.4 MeV $^4He^{++}$. The highlighted region in the PIXE spectrum was used for normalization (see text for further details).
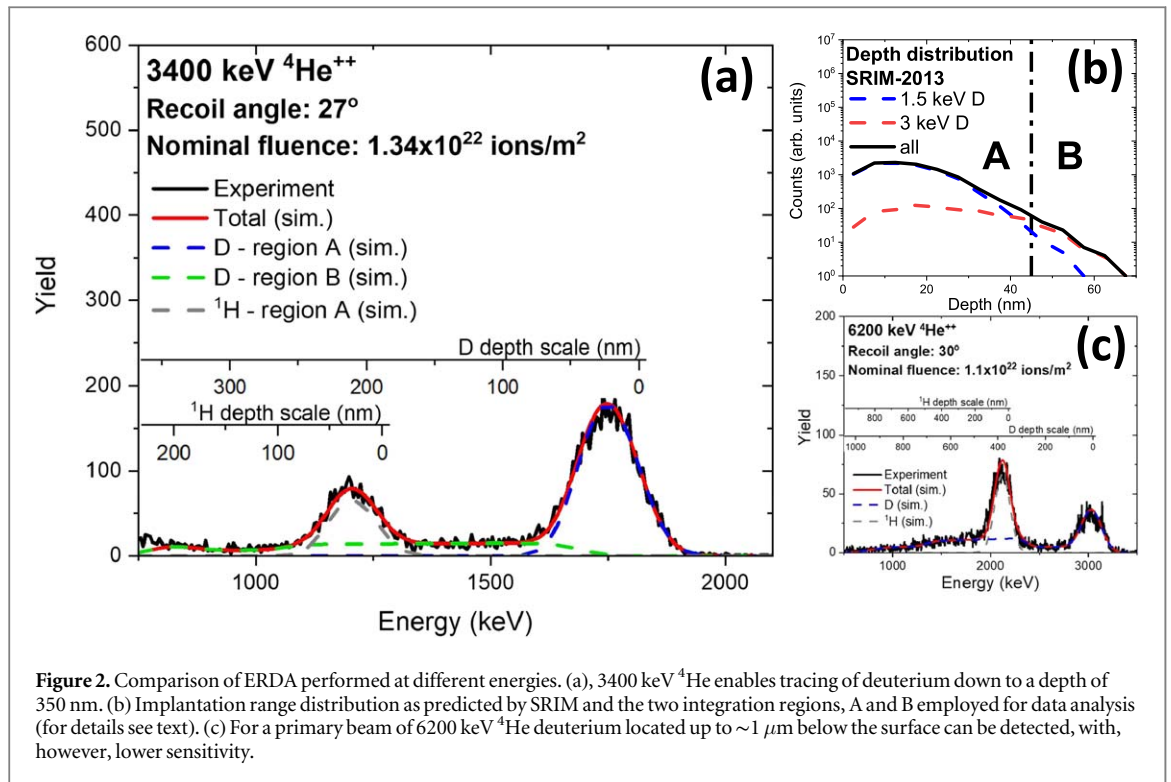
PIXE spectra were recorded simultaneously with ERDA, using a Silicon Drift Detector (SDD) with an energy resolution of 0.136 keV for the Fe–K_α characteristic energy and a solid angle of $(3.3 \pm 0.2) \times 10^{-3}$ Sr, placed at an angle of 135° with respect to the beam direction. A mylar foil of 204 μm thickness was placed in front of the x-ray detector to prevent backscattered particles hitting the detector and to reduce pile-up contribution in the electronics from Bremsstrahlung and excessive characteristic x-rays from tungsten L (and M) lines.

For sample annealing we used an electron beam heater, which was automatically controlled by a VG Scienta electron beam heating controller. Sample heating was controlled via a K-type thermocouple in contact to the surface of the sample and the temperature was recorded simultaneously with signals from IBA and RGA (panel b). The temperature reading was corrected by making use of an optical pyrometer (Micro-pyrometer PV 11-Keller HCW GmbH) to calibrate sample temperature at elevated temperatures. Samples were annealed up to $\approx$1400 K in in a stepwise ramp mode (100–200 K per step) with IBA spectra recorded at each step. The base pressure during the entire *in-situ* procedure (ion implantation, sample annealing, IBA and TDS) was lower than 1×10^{-8} mbar.

For the TDS, the RGA was set to record the partial pressure of species with a mass of 4 amu (corresponding to D_2) during annealing and simultaneously with IBA. A plot showing the pressure of deuterium as a function of time during annealing is shown in figure 1(b).

Figure 1 also presents a comparison of several ERDA (panel c) and PIXE (panel d) spectra obtained during the annealing ramp ranging from 306 K to $\sim$1360 K. The deuterium implanted in the sample and protium at the sample surface form two well separated peaks in the ERDA spectrum, while the tungsten L-lines are detected by PIXE. Both ERDA and PIXE spectra are normalized by the respective accumulated charge of each measurement. The primary beam current was measured by a Faraday Cup before and after each measurement, while fluctuations of the current during the measurement were tracked by changes in the PIXE W-L_α signal indicated by the highlighted region in the panel (d) spectra. As the PIXE yield from W-L_α is proportional to the beam current [36], this yield was always used to normalize hydrogen concentrations in the following for quantitative analysis. Deuterium and surface protium release at elevated temperatures is indicated by the decrease of detected recoils (panel c).
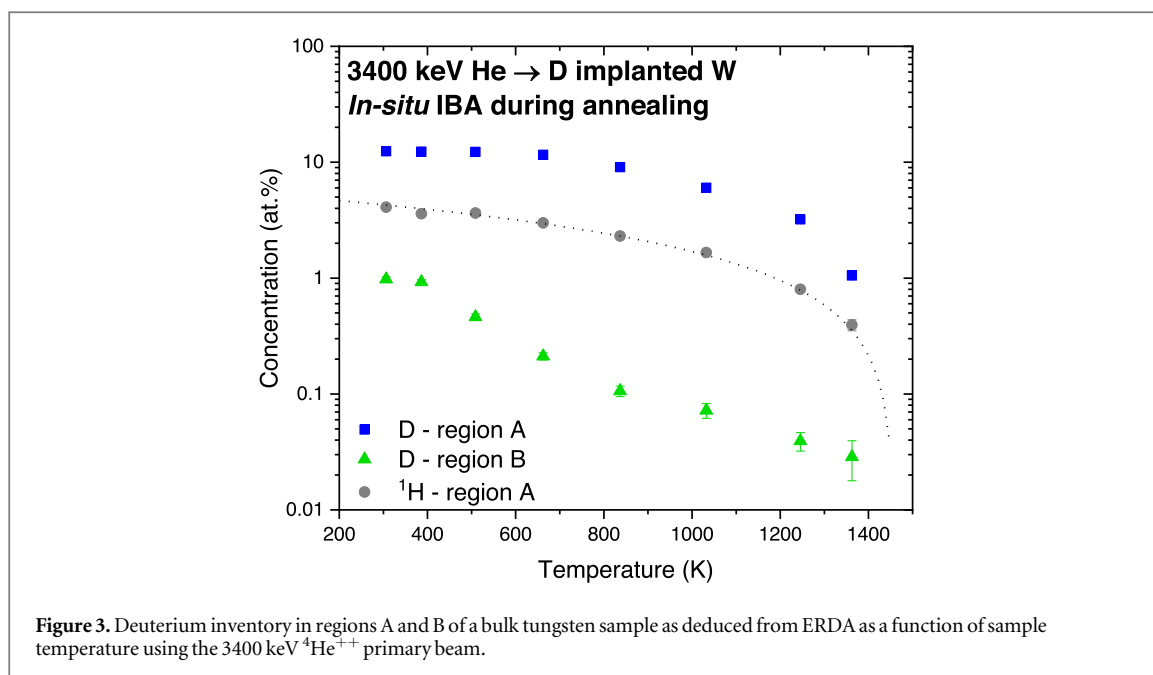
For quantitative analysis, ERDA spectra were fitted using the latest version of SIMNRA [37] and stopping power values from the latest version of SRIM [33]. The scattering cross-section for protium was retrieved from SigmaCalc [38]. For deuterium, we have measured the relative cross section at 27° and compared it to published

Figure 2. Comparison of ERDA performed at different energies. (a), 3400 keV ^{4}He enables tracing of deuterium down to a depth of 350 nm. (b) Implantation range distribution as predicted by SRIM and the two integration regions, A and B employed for data analysis (for details see text). (c) For a primary beam of 6200 keV ^{4}He deuterium located up to ∼1 μm below the surface can be detected, with, however, lower sensitivity.

values at 30° [34, 35]. A similar fit function as described in [35] was applied and no resonances were observed at the energies used in this work.

3. Results and discussion

For a quantitative evaluation of data obtained from ERDA, experimental spectra (shown in figure 1(b)) were split in different regions of interest. This selection permits to study the temperature dependence of the hydrogen inventory for different types of retained hydrogen. Apart from the distinct peaks that correspond to protium and deuterium in the near-surface region, the tail on the left side of the deuterium peak indicates D diffused deeper into the material. ERDA performed on virgin samples revealed only small amounts of protium below the sample surface (<0.1 at.%-not shown). The expected range distribution for atomic and molecular species from implantation can be predicted by SRIM-2013 (see figure 2(b)). For the present conditions, the projected ion ranges do not exceed ≈45 nm. Based on these results, for quantification of the D-inventory, we defined a near-surface region (region A) containing implanted particles as well as surface deuterium and a second region (region B) that corresponds to the bulk of the sample, where diffused deuterium is detected. The border between these two regions is illustrated in figure 3(b) (dashed line). The areal density of W in region A is 3×10^{17} atoms cm^{-2} and that of region B 1.8×10^{18} atoms cm^{-2}, the latter corresponding to 285 nm of bulk tungsten. The thickness of region B was determined by the detectable diffused deuterium, i.e. the probing depth of ERDA. From the separation in two regions and individual species, quantitative depth profile reconstruction was achieved using the software SIMNRA, which yielded the simulated spectrum visualized in figure 2(a). For the spectrum measured with 3400 keV ^{4}He^{++} presented in figure 2(a) (implantation dose of 1.34×10^{22} atoms m^{-2}), deuterium contents of regions A and B are 4.5×10^{20} atoms cm^{-2} (12.5 at.%) and 1.6×10^{20} atoms m^{-2} (1 at.%) respectively. Region B be can be further divided in two parts: energies above and below the protium peak. To make sure that the signal is exclusively attributed to deuterium, we tracked the signal between the two main peaks during annealing. The total amount of detected deuterium in both regions is 4.5% of the implanted dose, in good agreement with retention levels observed in other studies [39, 40]. As in earlier studies, we also observed blister formation (see Supplementary material (available online at stacks.iop.org/PS/96/124004/mmedia) for SEM-investigations), but preclude extensive trapping of deuterium beyond the range probed by ERDA [40, 41]. Figure 2(c) holds an ERDA spectrum of another implanted sample (fluence of 1.1×10^{22} ions m^{-2}), recorded at higher beam energy (6200 keV ^{4}He^{++}) and a recoil angle of 30°, which demonstrates how the depth profiling capability of ERDA scales with energy. This dataset, furthermore shows, that no large concentrations of trapped D have to be expected at larger depths. Note, however, that at present, recoil cross sections at such high energies are scarce and generally found lower than at more canonical energies.

Figure 3. Deuterium inventory in regions A and B of a bulk tungsten sample as deduced from ERDA as a function of sample temperature using the 3400 keV ^{4}He^{++} primary beam.

The consequently required higher beam energies and/or longer data acquisition times can be detrimental in combination with TDS analysis. In addition to the above-mentioned difference in depth resolution, this rendered the 3400 keV ERDA option more attractive for the present study.

To check for a possible ion-beam-induced release of hydrogen species, ERDA spectra (see supplementary information) were recorded for the sample at room temperature using list-mode acquisition for in total 600 s. The total amount of deuterium and protium in the regions A and B of the sample was determined as a function of different integrated doses. No hydrogen release induced by the primary ion beam was detected throughout the measurement. This observation is also in accordance with TDS results, as no increase in D$_2$ partial pressure was recorded.
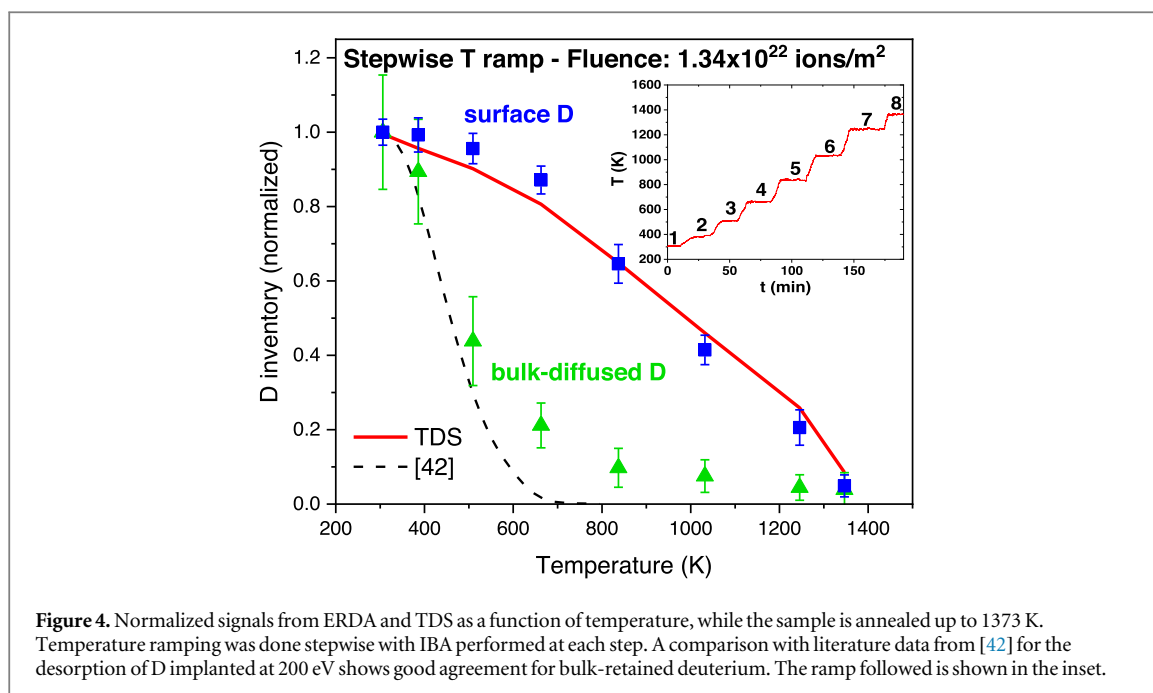
In the following, we analyze the results from the temperature ramping combining ERDA and residual gas analysis. ERDA was performed at eight temperature steps from room temperature up to $\approx$1373 K. The temperature increase between steps was automatically regulated within an annealing rate of 20 to 25 K min^{-1} (100-200 K step^{-1}). Temperature was kept constant at each step during IBA and data acquisition lasted for 10 to 15 min per step, needed to both minimize the statistical error and track the deuterium evolution over time at a specific temperature.

The atomic concentration of deuterium and protium in these two regions as a function of temperature are depicted in figure 3. Initially, the total deuterium integrated within region A (blue squares) is found to be 12.4 at.%, while in region B (green triangles) it does not exceed 1 at%. After remaining constant at the initial plateau extending up to about 400 K, the amount of deuterium in the bulk is decreasing in an approximately exponential manner with increasing temperature. In contrast, deuterium located in region A shows a different behavior. Initially, concentrations stay almost constant up to a temperature of $\approx$650 K, before a significant decrease can be observed. The decrease of surface protium shows an almost linear dependence on temperature (dotted line corresponding to a linear fit to guide the eye).

In figure 4, the normalized deuterium signal from the different inventories is shown in a linear scale as a function of temperature. This figure furthermore presents the TDS signal (red continuous line), which was recorded simultaneously to ERDA. TDS results were obtained by subtracting the background contribution from the RGA signal, integrating it over time and correlating the maximum value to the integral yield of desorbed deuterium. The inset of figure 4 shows the heating ramp with individual temperature steps noted by numbers.

Note, that the normalized TDS results show a very similar time and temperature dependence than observed for deuterium released from region A. No pronounced narrow desorption peaks have been detected.

Based on the experimental observations, we can draw a series of conclusions. The two different species of deuterium identified show a distinct behavior during the annealing process, which is clearly captured by the depth-resolved ERDA measurements. The dissolved deuterium (from deeper regions) is outgassing in an exponential manner, which can be understood from diffusion in the material. As shown in figure 3(b), region B is mostly beyond the implantation range of the implanted D ions. Similarly, the formation of ion-induced defects, which can act as trapping-sites will be negligible for region B. The de-trapping behavior from the deeper regions can be compared to previous investigations of low-energy D implantation in W. For example,

Figure 4. Normalized signals from ERDA and TDS as a function of temperature, while the sample is annealed up to 1373 K. Temperature ramping was done stepwise with IBA performed at each step. A comparison with literature data from [42] for the desorption of D implanted at 200 eV shows good agreement for bulk-retained deuterium. The ramp followed is shown in the inset.

Ogorodnikova *et al* performed TDS measurements of D implanted at 200 eV [42], which is an energy that is too low to form any vacancies in W at reported minimal displacement energies of close to 40 eV [43]. Their results of the observed D desorption behavior are included in figure 4 as the black dashed line. This comparison shows a good agreement with the D de-trapping in the bulk region, showing nicely how ERDA allows to deduce the D retention behavior in undamaged W deeper in the bulk at the same time as in the damaged regions closer to the surface.

In such regions, where ion-induced displacements were created, the stronger bonds of the near surface species initially result in a threshold-like behavior that is followed by a linear decrease in the signal. Interestingly, the TDS signal shows a similar behavior. At the same time, the TDS-signal is expected to comprise the integral D-release from near-surface damage sites, interstitial sites and blister regions. The combination of TDS and IBA thus permits to extract additional differential information, confirming only a limited amount of D being retained in subsurface blisters due to the total amount of D detected by IBA. As described in figure 3, the D in both ERDA regions does not exceed 5% of the total nominal implanted dose. The diffusion of dissolved D to the surface is, as evidenced by ERDA, not expected to significantly contribute to the TDS-signal at elevated temperatures. The results also demonstrate, that protium, which is physi- and chemisorbed to the surface, exhibits linearly decreasing concentration for increasing temperatures.

4. Summary and conclusions

Here, we presented a complete *in-situ* experimental procedure that included deuterium implantation in tungsten, followed by TDS and simultaneous protium and deuterium profiling by IBA. The demonstrated approach allows for quantitative, depth and isotope resolved analysis of the retention of fuel species in plasma facing components at different temperatures, relevant for development of fusion devices. As a well-studied reference system, we chose deuterium-implanted polycrystalline tungsten. The hydrogen inventory in tungsten bulk samples during annealing was reconstructed from simultaneously performed ERDA and TDS. Depth-resolved ERDA results allowed us to make a distinction between the deuterium trapped in near-surface defects and deuterium dissolved and diffused deeper in the material. The evolution of these inventories with temperature was found to be different in agreement with previous studies on deuterium retention in tungsten. For deuterium and protium located close to surface, no preferential release peaks are observed. The behavior of deuterium diffused deeper in the material suggests that interstitial deuterium atoms present higher mobility at lower annealing temperatures, in contrast to deuterium atoms trapped in defects in the implantation region in accordance with different trapping energies, as expected. The combination with TDS allows to extract additional differential information on deuterium retained deeper in defects and blisters formed along grain boundaries. The *in-situ* simultaneous operation of the two techniques makes the present approach also attractive for *in-situ* investigation of deuterium retention in other PFCs (as e.g., beryllium). To further increase the relevance of

results from such studies for operation of fusion devices, an upgrade of the implantation system, allowing for a wider range of fluxes and fluences is desirable.
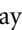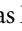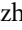
Acknowledgments

Data availability statement

The data generated and/or analysed during the current study are not publicly available for legal/ethical reasons but are available from the corresponding author on reasonable request.

ORCID iDs

K Kantre ⬚ https://orcid.org/0000-0002-0077-2620
P S Szabo ⬚ https://orcid.org/0000-0002-7478-7999
M V Moro ⬚ https://orcid.org/0000-0003-4334-7461
C Cupak ⬚ https://orcid.org/0000-0003-4502-5749
R Stadlmayr ⬚ https://orcid.org/0000-0001-5194-1933
L Zendejas Medina ⬚ https://orcid.org/0000-0002-9204-5999
F Aumayr ⬚ https://orcid.org/0000-0002-9788-0934
D Primetzhofer ⬚ https://orcid.org/0000-0002-5815-3742

References

[1] Naujoks D 2006 *Plasma-Material Interaction in Controlled Fusion* 1st Edn (Berlin : Springer) (https://doi.org/10.1007/3-540-32149-7)
[2] Federici G *et al* 2001 Plasma-material interactions in current tokamaks and their implications for next step fusion reactors *Nucl. Fusion* **41** 1967–2137
[3] Brezinsek S *et al* 2017 Plasma-wall interaction studies within the EUROfusion consortium: Progress on plasma-facing components development and qualification *Nucl. Fusion* **57** 116041
[4] Linsmeier C, Reinelt M and Schmid K 2011 Surface chemistry of first wall materials - From fundamental data to modeling *J. Nucl. Mater., Elsevier B.V.* **415** S212
[5] Kurnaev V A, Matveev D I and Trifonov N N 2007 Simulation of charge exchange neutrals interactions with gaps in first wall cladding *J. Nucl. Mater.* **363–365** 797–800
[6] Tanabe T 2014 Review of hydrogen retention in tungsten *Phys. Scr.* **T159** 014044
[7] Pardanaud C *et al* 2015 Hydrogen retention in beryllium: Concentration effect and nanocrystalline growth *J. Phys. Condens. Matter* **27** 475401
[8] Hirai T *et al* 2013 *ITER Tungsten Divertor Design Development And Qualification Program* (North-Holland: Fusion Eng. Des.) pp 1798–801
[9] Eckstein W, Garcia-Rosales C, Roth J and Ottenberger W 1993 Sputtering data *Max-Planck-Institut für Plasmaphysik* **IPP 9/82** IPP report (hdl.handle.net/11858/00-001M-0000-0027-6326-2) (accessed March 11, 2020)
[10] Sugiyama K, Schmid K and Jacob W 2016 Sputtering of iron, chromium and tungsten by energetic deuterium ion bombardment *Nucl. Mater. Energy.* **8** 1–7
[11] Likonen J, Heinola K, De Backer A, Baron-Wiechec A, Catarino N, Jepu I, Ayres C F, Coad P, Matthews G F and Widdowson A 2019 Investigation of deuterium trapping and release in the JET divertor during the third ILW campaign using TDS *Nucl. Mater. Energy.* **19** 300–6
[12] Maier H, Schwarz-Selinger T, Neu R, Garcia-Rosales C, Balden M, Calvo A, Dürbeck T, Manhard A, Ordás N and Silva T F 2019 Deuterium retention in tungsten based materials for fusion applications , *Nucl. Mater. Energy.* **18** 245–9
[13] Baldwin M J, Doerner R P, Wampler W R, Nishijima D, Lynch T and Miyamoto M 2011 Effect of He on D retention in W exposed to low-energy, high-fluence (D, He, Ar) mixture plasmas *Nucl. Fusion* **51** 103021
[14] Ogorodnikova O V, Roth J and Mayer M 2008 Ion-driven deuterium retention in tungsten *J. Appl. Phys.* **103** 034902
[15] Oya Y, Li X, Sato M, Yuyama K, Oyaidzu M, Hayashi T, Yamanishi T and Okuno K 2016 Deuterium permeation behavior for damaged tungsten by ion implantation *J. Nucl. Sci. Technol.* **53** 402–5
[16] Markelj S, Založnik A, Schwarz-Selinger T, Ogorodnikova O V, Vavpetič P, Pelicon P and Čadež I 2016 *In situ* NRA study of hydrogen isotope exchange in self-ion damaged tungsten exposed to neutral atoms *J. Nucl. Mater.* **469** 133–44
[17] Nastasi E and Wang Y 2009 Handbook of Modern Ion Beam *Analysis, 2nd editio, Materials Research Society*

[18] Tal-Gutelmacher E, Eliezer D and Abramov E 2007 Thermal desorption spectroscopy (TDS)-Application in quantitative study of hydrogen evolution and trapping in crystalline and non-crystalline materials *Mater. Sci. Eng. A* **445–446** 625–31

[19] Eleveld H and van Veen A 1992 Deuterium interaction with impurities in tungsten studied with TDS *J. Nucl. Mater.* **191–194** 433–8

[20] Eichler M 2019 Investigation of hydrogen isotope retention mechanisms in beryllium: High resolution TPD measurements *Nucl. Mater. Energy.* **19** 440–4

[21] Sato K, Tamiya R, Xu Q, Tsuchida H and Yoshiie T 2016 Detection of deuterium trapping sites in tungsten by thermal desorption spectroscopy and positron annihilation spectroscopy , *Nucl. Mater. Energy.* **9** 554–9

[22] Yuan Y, Guo W, Wang P, Qu S, Liu W, Luo G-N, Cheng L and Lu G-H 2019 Influence of surface melting on the deuterium retention in pure and lanthanum oxide doped tungsten *Nucl. Fusion* **59** 016022

[23] Younkin T R, Biewer T M, Klepper C C and Marcus C 2014 Description of the prototype diagnostic residual gas analyzer for ITER *Rev. Sci. Instrum.* **85** 11E816

[24] Louthan M R and Derrick R G 1975 Hydrogen transport in austenitic stainless steel *Corros. Sci.* **15** 565–77

[25] Linsmeier C, Goldstraß P and Klages K U 2001 ARTOSS - A new surface science experiment to study the hydrogen inventory in multi-component materials *Phys. Scr. T* (Bristol: IOP Publishing) pp 28–33

[26] Založnik A, Markelj S, Čadež I, Pelicon P, Vavpetič P, Porosnicu C and Lungu C P 2015 The influence of nitrogen co-deposition in mixed layers on deuterium retention and thermal desorption *J. Nucl. Mater.* **467** 472–9

[27] Oberkofler M and Linsmeier C 2011 Deuterium release from implanted beryllium and beryllium oxide *J. Nucl. Mater., Elsevier B.V.* **415** S724–7

[28] Ström P, Petersson P, Rubel M and Possnert G 2016 A combined segmented anode gas ionization chamber and time-of-flight detector for heavy ion elastic recoil detection analysis *Rev. Sci. Instrum.* **87** 103303

[29] Kantre K, Moro M V, Moldarev D, Johansson D, Wessman D, Wolff M and Primetzhofer D 2020 SIGMA: a set-up for in-situ growth, material modification and analysis by ion beams *Nucl. Instruments Methods Phys. Res. Sect. B Beam Interact. with Mater. Atoms.* **463** 96–100

[30] Mayer M *et al* 2019 Ion beam analysis of fusion plasma-facing materials and components: Facilities and research challenges *Nucl. Fusion* **60** 025001

[31] Rapp D, Englander-Golden P and Beiglia D D 1965 Cross sections for dissociative ionization of molecules by electron impact *J. Chem. Phys.* **42** 4081–5

[32] Möller W 2014 TRI3DYN-collisional computer simulation of the dynamic evolution of 3-dimensional nanostructures under ion irradiation *Nucl. Instruments Methods Phys. Res. Sect. B Beam Interact. with Mater. Atoms.* **322** 23–33

[33] Ziegler J F, Ziegler M D and Biersack J P 2010 SRIM-The stopping and range of ions in matter (2010) *Nucl. Instruments Methods Phys. Res. Sect. B Beam Interact. with Mater. Atoms.* **268** 1818–23

[34] Han Z, Hao W, Wang C and Shi L 2016 Elastic recoil cross section determination of deuterium by helium-4 ions at 30° with the energy range of 2.6–7.4 MeV *Nucl. Instruments Methods Phys. Res. Sect. B Beam Interact. with Mater. Atoms.* **375** 13–6

[35] Kellock A J and Baglin J E E 1993 Absolute cross section for D(4He, D)4He forward scattering *Nucl. Inst. Methods Phys. Res. B.* **79** 493–7

[36] Johansson S A E and Johansson T B 1976 Analytical application of particle induced x-ray emission *Nucl. Instruments Methods.* **137** 473–516

[37] Mayer M 2008 SIMNRA, a simulation program for the analysis of NRA, RBS and ERDA in:*AIP Conf. Proc.* (AIP Publishing) pp 541–4

[38] Gurbich A F 2016 SigmaCalc recent development and present status of the evaluated cross-sections for IBA *Nucl. Instruments Methods Phys. Res. Sect. B Beam Interact. with Mater. Atoms.* **371** 27–32

[39] Nagata S and Takahiro K 2000 Deuterium retention in tungsten and molybdenum *J. Nucl. Mat. 283-* **287** 1038

[40] Taylor C N, Shimada M and Merill B J 2017 *Nucl. Mat. & Energy* **12** 689

[41] Balden M, Lindig S, Manhard A and You J H 2011 D2 gas-filled blisters on deuterium-bombarded tungsten *J. Nucl. Mater.* **414** 69–72

[42] Ogorodnikova O, Roth J and Mayer M 2003 Deuterium retention in tungsten in dependence of the surface conditions *J. Nucl. Mater.* **313** 469–77

[43] Maury F, Bidget M, Vajda P, Lucasson A and Lucasson P 1978 Frenkel pair creation and stage I recovery in W crystals irradiated near threshold *Rad. Eff.* **38** 53